Jordan Journal of Civil Engineering, Volume **11**, No. **2**, **2017**

The Effect of Base to Focal Length Ratio on Stereo Rig Calibration Using a Planar Constraint Facility

Mohammed Taleb Obaidat

Professor of Civil Engineering, Jordan University of Science and Technology (JUST), Irbid, P.O. Box 3030, Jordan. E-Mail: mobaidat@just.edu.jo

ABSTRACT

The effect of camera configuration; namely the base/focal length (*b/f*) ratio, on camera calibration parameters of a planar constraint facility was investigated. A planar calibration facility with 378 points 10 cm apart was constructed. A rolling platform that permitted variable base of stereo camera configuration, using one camera or two, was also designed. However, one camera was used for the stereo configuration utilized in this research work. Combinations of 11, 16, 25 and 45 mm focal settings and 40, 60 and 80 cm bases were used. This produced a range of *b/f* ratio ranging from 8.9 to 72.7. A mathematical algorithm and a software package were developed to calibrate hand-held Charge-Coupled-Device (CCD) cameras using a planar facility with four-distance control. A parametric study was carried out to investigate the b/f ratio effect on calibration parameters. Propagation of variance and covariance of unknown residuals of image point and control distance computations, least-square mathematical model efficiency and potential accuracy of 3-D measurement computations were used to investigate the efficiency of this study. Experimental results showed that using *b/f* ratio between 20 and 70 was the optimal mapping configuration that had the capability of modelling the entire interior geometry of camera lens and plane coefficients accurately, as well as precisely computing the standard deviation of unknowns. Increasing the *b/f* ratio would produce a shift and instability in the principal point, a decrease in the affine scaling parameter and stability in the decentering distortion parameters and number of iterations. Increasing the camera base at constant focal setting would decrease the standard deviations of calibration parameters and increase reliability of the computed 3-D coordinates.

KEYWORDS: Camera configuration, Camera calibration, Focal length, Scale, Base, Off-the-shelf vision systems, CCD-cameras, Planar constraints, Lens distortion.

INTRODUCTION

Camera calibration is the key to perform precise surface measurements for real-time and automated mapping. Its purpose is to reconstruct graphically, instrumentally or mathematically the precise passage geometry of the bundles of rays that entered the camera at the instant of exposure. The suitability and evaluation of calibration techniques in photogrammetry are still being under development. In the past two decades, scientists concentrated on geometric degradations. However, the radiometric degradation effect on geometric fidelity has to be examined yet. The trend of photogrammetric processing is rapidly going toward digital data acquisition systems, computer vision and on-line and real-time measurements (Kratky, 1989; Honda and Nagai, 2002; Wolf, 2002).

Real-time systems for metrology applications involve measurement of image coordinates, stereo

Received on 7/7/2015.
Accepted for Publication on 13/10/2015.

image correlation algorithm, reliable camera calibration procedure and three-dimensional (3-D) space coordinates' computation procedure. Image coordinates' measurement requires sub-pixel location accuracy algorithms, while 3-D space coordinates' computation requires stereo correspondence matching and intersection algorithm (Bleyer and Gelautz, 2005). However, camera calibration procedure requires rigorous, reliable and practical least square adjustment algorithm to compute interior and exterior orientation parameters. Therefore, automatic measurement and control of 3-D process from two-dimensional (2-D) metrology is a challenging photogrammetric expertise (El-Hakim et al., 1989).

Since photogrammetric cameras don't possess perfect lens systems, they have to be calibrated to model the passage of light rays through the lens and onto the image plane. Except in case of self-calibration method, the interior orientation parameters, including principal distance (focal distance), principal point and radial and decentering distortion of the lens, must be known before any camera system is used for photogrammetric projection. The key of having precise 3-D object space coordinates' computation is the usage of a precise camera calibration method. Obaidat and Wong (1996) and Obaidat and Al-Masaeid (1998) investigated thoroughly the usage of planar wall facility as a calibration facility for CCD-cameras. Their method showed great potential capabilities and feasibility for calibration task using different numbers of 3-D and distance controls. In fact, the maximum errors of image point residuals were constantly falling within (0.3-0.6) pixel. The method was also used extensively in metrology applications such as: restoration techniques, maintenance applications and construction and monitoring of historical monuments. However, Obaidat and Al-Masaeid (1998) recommended to extend the investigation of this method to study the factors of camera configuration (base to object distance ratio), image resolution, camera warm-up, as well as wave and deviation effects on interior and exterior calibration parameters.

In this paper, the effect of camera configuration; i.e., the base/focal length ratio, on camera calibration parameters using planar constraint facility was mainly investigated. Parametric study's effect on the potential accuracy of 3-D measurements and least square algorithm's efficiency will be determined. Moreover, propagation of variance and covariance will be used to evaluate the accuracy of the camera calibration parameters and computed 3-D surface measurement quantities within a least-square solution.

LITERATURE REVIEW

The trend in mensuration of non-topographic photogrammetry systems is going rapidly toward automation utilizing fully automated or off-the-shelf vision systems (Obaidat and Wong, 1996; Obaidat and Al-Masaeid, 1998; Abraham and Förstner, 2005). The spatial directions of objects could be recorded by a CCD-camera and then image measurements could be taken on-line or off-line in order to extract 3-D object coordinates using non-metric or semi-metric data reduction algorithms (Faig, 1989). However, vision system geometric fidelity, including: optical lens distortion, synchronization of Analog-to-Digital (A/D) geometric converter error, pixel location error, quantizing error and discrete picture elements (pixels) would affect the potential accuracy of the automated and real-time mapping systems for large-scale applications (Wong et al., 1989). A measurement accuracy of less than (0.1-0.2) pixel size is nowadays achieved. However, several factors affect the potential accuracy of any developed vision system, including: stereo-camera configuration and setup, camera type and format, digitizing resolution, digitizing accuracy and repeatability, definition of interior orientation parameters, lightening system and contrast, stereo-image correlation and recognition, data-acquisition system stability, 3-D reconstruction, image scale and camera calibration procedure reliability. Therefore, interior and exterior camera calibration parameters should be found using a reliable method in order to

maximize the confidence and trust of the extracted surface measurements using stereovision systems.

Camera calibration is commonly carried out using one of the following methods: laboratory calibration, on-the-job calibration, self-calibration, analytical plumb line, finite element or planar object facility (Fryer, 1989; Obaidat and Wong, 1996). The test range laboratory calibration field commonly includes (50-100) accurately surveyed 3-D target points randomly located in (3-7) planes. The 3-D coordinates of the laboratory calibration targets are found using the intersection algorithm after measuring the horizontal and vertical angles to the targets from two control points connected by a reference line. The mapped object could then be mapped using the calibrated camera by applying the intersection algorithm developed from collinearity equations (Faig, 1989). In on-the-job calibration method, the solution is based on a sufficiently large number of well-distributed control points laid on a movable calibration facility. The camera or stereo camera location would be stationary to map the calibration facility and the object simultaneously. Thus, the calibration field image would be used for calibration and the other image would be used for measurement of the mapped object. In case of self-calibration method, which does not require object-space control except for the actual object evaluation (minimum of two horizontal and three vertical controls), the photography of both the object and the object-space control would be utilized to find camera calibration parameters as well as the unknown surface 3-D object points. Self-calibration could be considered as a recent bundle adjustment program. Therefore, it would be used in industrial and engineering applications using convergent photography (Fraser and Veress, 1980).

Brown (1971) stated that the plumb-line calibration method involves photographing a set of plumb-lines arrayed in the desired object plane and exploits the fact that in the absence of distortion, the central projection of a straight line is itself a straight line. Thus, systematic deviations of the images of plumb-lines from straight lines are due to distortion effect. Thus, plumb-line calibration method computes lens distortion parameters only.

The finite-element approach of camera calibration divides the image plane into finite elements. The image plane domain might be divided into rectangular, triangular or square elements. The main assumption of this approach is to consider a different focal length for each element on the photograph domain. Therefore, there would be no lens distortion coefficients as in the self-calibration method.

The planar calibration facility method was introduced by Obaidat and Wong (1996) and studied thoroughly by Obaidat and Al-Masaeid (1998). The concept of this method is based on enforcing the bundle of stereo rays acquired by a CCD-camera to intersect at a planar constraint facility. In case of the absence of geometric distortion, the coplanar bundles of rays are enforced to intersect at the planar constraint object. The key advantages of this method include: the availability of planar constraints in all buildings without the need of control survey, the capability of zooming for full range of focal setting and the usage of nominal focal settings. Further, a planar object could allow setting up perspective or grid homography between the left image and the right image (Pekelsky and Wijk, 1989). This method showed higher potential and effectiveness than 3-D laboratory field calibration, especially for large focal setting (Obaidat and Wong, 1996). In this paper, a parametric study is conducted to investigate different parameters related to camera calibration; including: camera configuration (*b/f)* ratio, least-square algorithm's efficiency, propagation of variance and covariance and potential accuracy of 3-D measurements. The paper focuses on finding the optimal base to focal length configuration to calibrate a CCD-camera and measure a planar object.

GEOMETRY OF PHOTO-COORDINATE SYSTEM

The geometry of the 3-D photo-coordinate system $(\bar{x}, \bar{y}, \bar{z})$ with respect to the exposure center (O) is shown in Figure 1. The principal point position on the image plane is defined by its coordinates (x_p,y_p); i.e., the

intersection point of the perpendicular line generated from (*O*) to the image plane. This perpendicular distance is always constant for every photograph and is called the focal length (*f*). Since fiducial points are not always perfectly aligned, the intersection of the opposite fiducial points (*O`*) would not be in coincidence with the principal point location. Therefore, the intersection of the opposite fiducial points forms the 2-D perpendicular image axes (*x* and *y*). Introducing the geometric lens symmetrical distortion coefficients (l_1 and l_2) and the asymmetrical distortion coefficients (p_1, p_2 and p_3), as well as corrections for geometric lens distortion ($\Delta x_a, \Delta y_a$), the corrected location $(\bar{x}'_a, \bar{y}'_a, \bar{z}'_a)$ of any image point, such as (x_a, y_a), could be defined as in the following equations (Wong, 1980):

$$\bar{x}'_a = (x_a - x_p)(1+k) + \Delta x_a \quad (1)$$

$$\bar{y}'_a = (y_a - y_p) + \Delta y_a \quad (2)$$

$$\bar{z}'_a = -f \quad (3)$$

where

$$\Delta x_a = (x_a - x_p)\left[l_1 r^2 + l_2 r^4\right] + \left[p_1(r^2 + 2(x_a - x_p)^2) + 2p_2\left(x_a - x_p\right)(y_a - y_p)\right] * \left[1 + p_3 r^2\right] \quad (4)$$

$$\Delta y_a = (y_a - y_p)\left[l_1 r^2 + l_2 r^4\right] + \left[p_2(r^2 + 2(y_a - y_p)^2) + 2p_1\left(x_a - x_p\right)(y_a - y_p)\right] * \left[1 + p_3 r^2\right] \quad (5)$$

r is the diagonal distance between principal point and image point and (*k*) is the affine scaling parameter of vertical and horizontal ratio of image pixels.

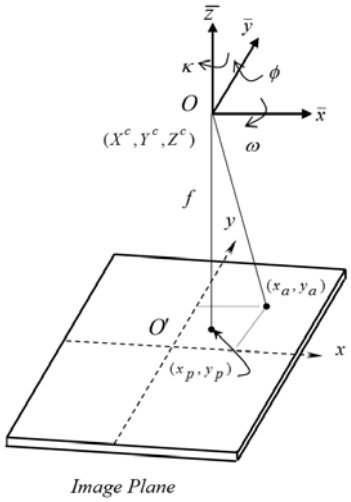

Figure (1): Geometry of 3-D photo-coordinate system

The parameters (x_p, y_p, *f*, *k*, l_1, l_2, p_1, p_2, p_3) represent the interior orientation parameters of the camera lens. The spatial position of the exposure center is defined by its coordinates (X^c, Y^c, Z^c) and the direction of the optical axis might be defined by the rotation angles (ω, ϕ, κ) about the ($\bar{x}, \bar{y}, \bar{z}$) axes, respectively. The

three spatial positions of the exposure center and the three rotation angles represent the exterior orientation parameters. The collinearity equations that form the relationship between photo coordinates (x_a, y_a) and their respective ground coordinates (X_A, Y_A, Z_A) could be represented by:

$$x_a + \Delta x_a - x_p + f\frac{\left[m_{11}(X_A - X^C) + m_{12}(Y_A - Y^C) + m_{13}(Z_A - Z^C)\right]}{\left[m_{31}(X_A - X^C) + m_{32}(Y_A - Y^C) + m_{33}(Z_A - Z^C)\right]} = 0 \quad (6)$$

$$y_a + \Delta y_a - y_p + f\frac{\left[m_{21}(X_A - X^C) + m_{22}(Y_A - Y^C) + m_{23}(Z_A - Z^C)\right]}{\left[m_{31}(X_A - X^C) + m_{32}(Y_A - Y^C) + m_{33}(Z_A - Z^C)\right]} = 0 \quad (7)$$

where m_{ij} is function of three rotation parameters (ω, ϕ, κ).

GEOMETRY AND CONDITION EQUATIONS

The basic solid analytical geometry of object space coordinate systems in photogrammetry is to consider perpendicular and right-handed coordinate axes. Therefore, the positive direction on angular measurement appears to be counter-clockwise. For a planar calibration facility, the object space coordinates of a plane (*X,Y,Z*) that passes through any control point such as (*i*) of coordinates (X_i, Y_i, Z_i) are located on the calibration plane and have directional numbers or plane parameters (A, B, C) that could be written as:

$$A(X - X_i) + B(Y - Y_i) + C(Z - Z_i) = 0 \quad (8)$$

In case of the absence of geometric distortion, the coplanar bundles of rays are enforced to intersect at the planar constraint object. Therefore, when stereo photographs are taken for the planar object, the object space coordinates of any point (*X, Y, Z*) on the mapped planar object could be written as function of measured image coordinates, distortion and affine scaling parameters, exterior orientation parameters and nominal focal length value (Equations 6 and 7) (Wong, 1980).

To control the scale of mapping, distance control should be used. In this study, only four distances measured on the planar object were used to assure correct determination of image scale. The four distances were meant to be the diagonal distances connecting four evenly distributed corner points and the center of the mapped planar wall facility. Four 3-D coordinate control points on the planar wall were also used to compute the initial values of plane parameters.

The distance observation equations could be also written as function of (*X, Y, Z*) of the selected points. Therefore, the least-square compacted symbolic form of the produced condition equation could be written in the following matrix form:

$$\overline{A}_{(m+4,4m+4)}V_{(4m+4,1)} + \overline{B}_{(m+4,15)}\Delta_{(15,1)} = \overline{\mathrm{E}}_{(m+4,1)} \quad (9)$$

where matrices $\overline{A}$, *V*, $\overline{B}$, Δ *and* $\overline{\mathrm{E}}$ represent the residual coefficients' matrix, the residual matrix, the unknown coefficients' matrix, the vector matrix of 15 unknowns and the discrepancy matrix, respectively, while (*m*) is the number of points on the planar wall appearing on the stereo images.

The 15 unknowns of the least-square model include five distortion parameters, the principal point coordinates, the affine scaling parameter, the parameters of the planar wall and the rest of the exterior orientation parameters of the calibrated camera at the right position (denoted as super *r*) exposure center of the stereo camera setup (X^{cr}, $\omega^r, \phi^r, \kappa^r$). The six exterior orientation

parameters of the left camera position (denoted as super *l*) and the (Y^r, Z^r) of the right position of the camera were found using approximated coordinates of one point located at each of the four corners of the planar facility, assuming an arbitrary coordinate system for the plane with camera base in the X-axis of the plane. Equation (9) could be easily solved using an iterative normal equations' representation.

The variance-covariance matrix (σ_Δ) of the solution of (Δ) may be computed using the following expression:

$$\sigma_\Delta = \sigma_o^{\,2}\left[\overline{B}^T(\overline{A}W^{-1}\overline{A}^T)^{-1}\overline{B}\right]^{-1} \quad (10)$$

where σ_o, W and *T* are the standard error of unit weight matrix, the weight matrix and the matrix transpose symbol, respectively.

The variance-covariance matrix (σi) of point (*i*) for the computed (*X,Y,Z*) coordinates could be computed as follows:

$$\sigma i = \begin{bmatrix} \sigma^2{}_x & \sigma_{xy} & \sigma_{xz} \\ \sigma_{xy} & \sigma^2{}_y & \sigma_{yz} \\ \sigma_{xz} & \sigma_{yz} & \sigma^2{}_z \end{bmatrix} \quad (11)$$

COMPUTER SOFTWARE DEVELOPMENT

The developed mathematical model was translated into a computer package software using the C-language that combined the cognitive and interpretive skills of a human operator with computer power computational capabilities. The input files of the software consisted of stereo image coordinates, the four control distances, the initialization of camera calibration parameters, as well as the initialization of weights for parameters, image points and control distances. The program algorithm then initialized the normal matrices and took the contribution of image points and distances on planar object in a cumulative manner. As any least-square algorithm, the program formed the reduced normal equations and solved for corrections of unknowns using an automated and iterative convergence criterion (Felus, 2004).

The program's output included: the camera interior and exterior calibration parameters the variance-covariance matrices of all computed parameters, the residuals of parameters, stereo image points and controls with their associated statistical parameters, plane parameters, number of iterations for convergence and chi-square value at the associated degree of freedom, the computed standard error of unit weight and the 3-D coordinates on the planar object with their respective estimated standard deviations utilizing the intersection algorithm.

The program computed general information data such as: number of linearized coplanarity equations of all calibrated targets, number of observation equations and degree of freedom knowing the convergence criterion and deletion factor for observations having blunder errors.

CAMERA'S SETUP AND CALIBRATION FACILITY

For the implementation of this research work, a planar wall facility, shown in Figure 2, was constructed. It represents a planar object in the Surveying and Photogrammetry Laboratory at Jordan University of Science and Technology (JUST), Jordan. The targeted object points on the planar wall, which were 10 cm apart, were marked and numbered from 1 to 378. The used calibration wall was deviated less than 5 mm from the nominal plane.

A stereo camera rolling platform setup, shown in Figure 3, was designed and implemented for the purpose of this work. The platform, made of steel, permitted to mount stereo camera configuration at variable base distances. It also could be moved to capture in site camera calibration images. For stability purposes of the platform, the maximum allowable base was one meter. Calibration images of the used CCD-camera were captured having the stereo platform facing the planar wall calibration facility with the camera's optical axis approximately perpendicular to the nominal plane of the wall and the platform's base parallel to the X-axis of the assumed right-handed coordinate system of the plane.

It has to be noted here that one CCD-camera for the stereo configuration was used in the calibration process in order to find its calibration parameters. However, two cameras were shown in Figure 3 to demonstrate stereo camera setup mount for the designed variable base distance platform.

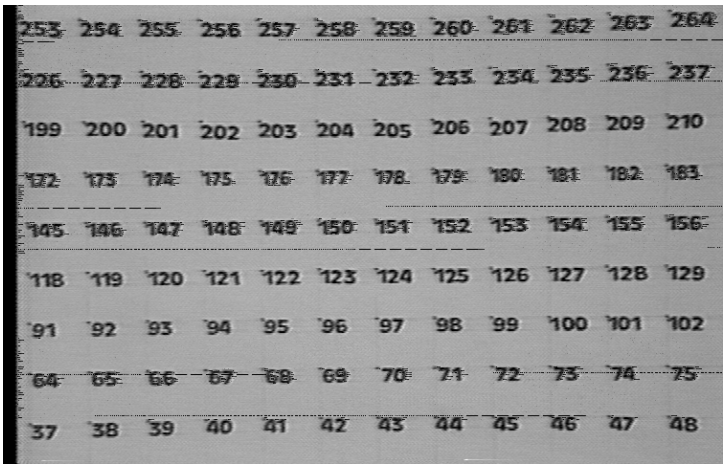

Figure (2): An image of the planar object used for camera calibration

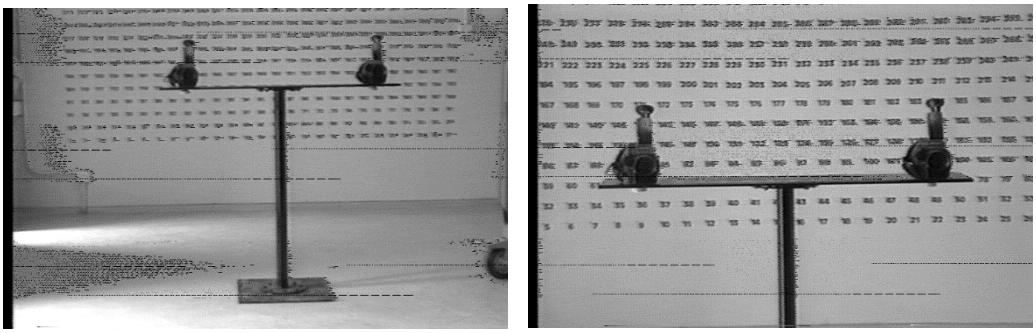

Figure (3): Stereo camera setup mounted on a rolling platform

BASE TO OBJECT DISTANCE RATIOS

Increasing the base to depth ratio for normal or convergent photography would increase the parallactic angle and the scale of the image. Therefore, image measurement would be much reliable and 3-D coordinates' precision would be enhanced, because it is function of the image coordinates' accuracy and camera resolution. Thus, the usage of different base to object distance ratios along with convergent photography was utilized in this study in order to investigate their effect on camera calibration parameters. Despite difficulties to produce visualized 3-D stereo images, the convergent photography increased the base to height ratio. In fact, there was no need for 3-D visualization, because computational algorithms were used to compute surface coordinates and parameters.

The zoom capability of the used CCD-cameras made it possible to use the focal length as an indicator of the object distance, because it is well known that decreasing the focal length or increasing the object distance would produce the same scale of the image. For this reason, the base to focal length ratio was used instead of the focal length to object distance ratio. In this study, 11, 16, 25

and 45 mm focal lengths and 40, 60 and 80 cm base values were used in order to study the potential effect of base to object distance ratio on calibration parameters. These values produced base to focal length values ranging from 8.9 (i.e., 40 cm / 45 mm) to 72.7 (i.e., 80 cm / 11mm).

However, it has to be noted that changing the focal length only and keeping the base unchanged would change the base to focal length ratio without changing the intersection geometry (distance to the object and convergence angle). Thus, *b/f* ratio was not anticipated to change the calibration parameters that much, but merely their variances by the image-scaling factor. To control mapping scale at every focal length, four measured distances on the planar object were used.

EXPERIMENTAL RESULTS

A nominal focal length value, which was found by calibrating the used CCD-camera once using a constructed 3-D laboratory calibration facility, was utilized in this work. Using a moderate focal setting of 28 mm and using the constructed 3-D laboratory calibration facility, it was found that 1mm focal setting was equivalent to 94.4 pixels on the image domain. Table 1 shows the focal settings used and their respective equivalent pixel values (based on that the nominal value of 1mm equals 94.4 pixels) and pixel sizes on the image domain (pixel size or scale changes for every focal setting).

A set of convergent stereo photographs that consisted of 12 images was captured at the studied range of focal settings for the constructed planar wall facility. The base (cm) and focal setting (mm) pairs used were: (40,11), (40,16), (40,25), (40,45), (60,11), (60,16), (60,25), (60,45), (80,11), (80,16), (80,25) and (80,45). The images were transferred into an available PC-based vision system in order to automatically convert their format into a digital one using an Analogue to Digital (A/D) converter. Images having the same focal setting were captured for all the possible used bases to assure the same accuracy among different exposures of the studied *b/f* ratios.

Table 1. Focal settings and their respective pixel values and sizes

f		Pixel Size on Image Domain (mm)
mm	**Pixels**	
11	1034	4.35
16	1504	2.99
25	2350	1.92
45	4230	1.06

Images were captured under sunlight condition using standard PAL resolution of 752 x 480 pixels at 256 gray levels using Samsung CCD camcorder equipped with zoom lens capability. Images were re-sampled to produce 512x512 pixels. The camera was equipped with an 8x powered zoom lens with a range of (8.5-68) mm.

The images were then processed and conjugate stereo image points automatically matched. Number of image points ranged from 16 to 66 depending on the focal setting values. Due to zooming process, the larger the focal setting the smaller the number of image points. The larger the number of stereo image points, the better would be the redundancy in the least-square model and thus it would affect the number of iterations as well as the standard error of unit weight. The camera resolution and using the corners of the 10 cm grids on the planar facility limited the number of targeted points. The developed calibration software was used to find the camera calibration parameters and plane parameters. The calibration parameters and planar wall facility

coefficients and their respective Root-Mean-Squares (RMS) for the full range of camera configuration; i.e., base to focal length settings, were computed. It was clear that the focus of this study was on the interior orientation calibration parameters and the planar wall coefficients. However, although the exterior orientation parameters were computed, they were neither reported here nor given that much concern. The reasons behind that were: 1) finding the interior calibration parameters would model the interior geometry of lens and the passage of light perfectly; and 2) approximated or initial values of exterior orientation parameters might give an excellent accuracy for these values due to setup constraints (base of stereo platform parallel to X-axis calibration facility) and eight out of twelve of exterior orientations had excellent initial approximation (only four unknowns X^{cr}, $\omega^r, \phi^r, \kappa^r$).

The statistics of residual error values of image coordinates used in the calibration process and their respective coefficients of variation (C.V.) for different camera configurations, showed that the maximum, mean and RMS of (*x*) and (*y*) residual errors of the image coordinates and the (*xy*) vector residual error are also varied. Similarly, Table 2 shows the maximum, mean and RMS of the four control distances used to scale the image configurations. The statistical values of the control distance residuals could be used as indicators of the effectiveness and superiority of the utilized calibration method.

Table 2. Control distance residuals for different camera configurations

Base (cm)	f (mm)	Distance Residuals (cm)			Number of Distances
		Maximum	Mean	σ Distance	
40	11	3.52 E-3	3.12 E-3	3.89 E-4	4
	16	3.29 E-3	1.19 E-4	2.36 E-3	4
	25	6.44 E-4	2.91 E-4	3.98 E-4	4
	45	5.23 E-4	7.79 E-5	4.22 E-4	4
60	11	1.28 E-3	2.02 E-4	9.25 E- 4	4
	16	1.63 E-3	1.54 E-4	1.32 E-3	4
	25	5.48 E-3	2.31 E-4	4.20 E-3	4
	45	2.23 E-3	1.02 E-3	1.08 E-3	4
80	11	2.37 E-3	6.55 E-5	1.79 E-3	4
	16	3.94 E-4	1.48 E-4	3.62 E-4	4
	25	1.31 E-3	2.85 E-4	6.97 E-4	4
	45	5.69 E-4	9.22 E-5	3.83 E-4	4

Table 3 shows the standard error of unit weight (σ_o) values and the number of iterations needed to converge the least-square adjustment mathematical model. For the studied camera configurations, the convergence criterion used was (0.1) pixel for a maximum allowable number of iterations of (100).

Table 3. Standard errors of unit weight and number of iterations for different configurations

Base (cm)	f (mm)	b / f	σ_0 (Pixel)	No. of iterations
40	11	36.4	0.656	32
	16	25.0	0.697	32
	25	16.0	0.484	10
	45	8.9	0.358	9
60	11	54.5	0.824	8
	16	37.5	0.627	6
	25	24.0	0.658	7
	45	13.3	0.972	13
80	11	72.7	0.649	14
	16	50.0	0.686	5
	25	32.0	0.666	4
	45	17.8	0.298	15

ANALYSIS AND DISCUSSION

Interior Orientation Parameters and Plane Coefficients

Table 2 shows the computed principal point coordinates, affine scaling parameters and the computed radial and decentering distortion parameters in pixels for the range of the camera configurations used. There was a shift in both principal point coordinates while changing the camera configuration. The shift in the x-direction was larger than that in the y-direction, because the spatial intersection provided the geometric distortion in the perpendicular line. In the x-direction, the shift amount in the principal point increased for higher values of base to focal length ratio. However, it fell consistently in the range of (0-11) pixels for the y-direction. There was no systematic pattern for the affine scaling parameter except that it decreased while increasing the base to focal length ratio. The reason behind that might be due to scale and base effects.

Regarding the standard deviations for principal point coordinates, affine scaling parameter and the first parameter of radial and decentering distortion, using the same focal setting and changing the base; i.e., *b/f* ratio is changed, the accuracy deviations for the interior orientation parameters would be changing. Increasing the base and using a constant focal setting; i.e., increasing the *b/f* ratio, would decrease the standard deviations of the computed interior orientation parameters. This could be used as an indicator of that increasing the *b/f* ratio would perfectly model the interior geometry of the lens and an optimal camera configuration could be known.

The stability of the principal coordinates was more for lower values of base to focal length ratio; i.e., higher focal setting at constant base or lower base at constant focal setting. This was due to geometry and scale effects. The pixel size ranged between 1.06 mm for focal setting of 45 mm and 4.35 mm for focal setting of 11 mm as shown in Table 1.

The radial distortion did not vary that much for different camera configurations. However, the change in the values of l_1 and l_2 for the studied base to focal length ratios was consistently less than ($4x10^{-06}$) and ($4x10^{-12}$) pixels, respectively. On the other hand, the base to focal length ratio had a significant effect on the decentering distortion. Increasing the base to focal setting ratio made the decentering distortion parameters more stable and reliable. After a base to focal length ratio of about (20-30), the decentering distortion parameters, especially p_2 and p_3, were almost constant regardless of the camera configuration. This might be used as an indicator to use

the base to focal length ratio (*b/f)* of (20-70) as the optimal mapping configuration. This optimal mapping configuration had the capability to model accurately the interior geometry of the lens.

The plane coefficients (A, B and C) showed a systematic trend for the effect of geometrical configuration on the calibration procedure. The coefficients were almost constant when increasing the values of *b/f* ratio. Again, *b/f* ratio of (20-70) was the optimal camera configuration to find consistent values of plane coefficients. Variations in B coefficient values; i.e., the depth direction coefficient, were due to the intersection geometry of bundles of rays on the planar object that was affected by the image scale and random errors in image coordinate measurement. It has to be noted that some unexpected results appeared for some of the computed parameters and coefficients, especially for large values of base and focal setting due to deviations of planar facility from the nominal plane.

Smaller values of *b/f* ratio of less than 20 showed an inconsistent geometric configuration fidelity for both distortion model and plane coefficients. That was due to instability of geometry and the great effect of the measured stereo image point accuracy on the computed parameters.

Residual Errors and Covariance in Image and Control Coordinates

The *b/f* ratio has an effect on the standard error of unit weight (σ_o), covariance of image coordinates and standard error of control distances. The σ_o value was affected by *b/f* ratios smaller than 20. However, it was consistent for *b/f* ratios in the range of (20-70). Similar trends were found for image coordinates' covariance and standard errors of control distances. The σ_o values were ranging between 0.298 and 0.972 pixel. This gave an indication of the measured accuracy of image coordinates that was about the same range (0.25-0.5 pixel). Enhancing the accuracy of the automatic target measurement procedure would improve the value of the standard error of unit weight. The covariance (σ_{xy}) of image coordinates for *b/f* ratios of (20-70) was less than 0.3 pixel. This implied that the mathematical calibration model eliminated the correlations between the computed parameters and the measured image coordinates. The RMS of control distances was in the range of (0.005-0.04) cm. However, for *b/f* ratios of (20-70), it was consistently in the range of (0.005-0.02) cm, which could be considered as a very small or negligible amount.

Mathematical Model Performance

The performance of any least-square algorithm could be measured using either the residuals of the measurements and the standard deviations of the unknowns or the time efficiency of the developed model. The previous section showed small amounts of residuals for control distances of less than 0.4 mm. Image residuals in both directions showed mean residuals in the range of (0.000006-0.0009) pixel. This could be an indicator of qualitative camera calibration model performance. However, the RMS of residuals in the y-direction showed lower values than in the x-direction due to the condition of spatial intersection that provided geometric condition to determine geometric distortion in the direction perpendicular to the column line (scan lines), while the planar object provided the geometric constraint along the row direction. Moreover, the planar facility had some more deviation from the nominal plane in the x-direction than in the y-direction.

The standard deviations of the unknown parameters including the interior distortion parameters and plane coefficients were computed. The standard errors of unknowns $(x_p, y_p, k, l_1, l_2, p_1, p_2, p_3, A, B, C)$ were relatively small as an indication of the algorithm's efficiency.

The number of iterations for the algorithm's convergence might be used as an indicator of its efficiency. Excluding the base of 40 cm, as the *b/f* ratio increased, the number of iterations fell consistently between 4 and 15. This means that the time efficiency of calibration method was high and the duration of running the software decreased consistently as the *b/f* ratio increased.

Moreover, validation of the least square model in Equation 9 has been carried out through forming new observations from the original ones. Adding the new observations to their respective residual values perfectly fulfilled the model and new residual values became exactly zero.

Standard Deviations of Computed 3-D Coordinates

Figure 4 shows the standard deviation values of the computed 3-D coordinates at a focal setting of 25 mm using camera bases of 40, 60 and 80 cm. This focal setting represented a moderate focal length value for the studied range. Increasing linear dependency exists between the standard deviation values for the computed coordinates in the Z-axis as the base is increased. However, it decreases linearly in case of Y-axis coordinates. The X-axis coordinates show no clear relationship. That was due to the geometrical strength of camera configuration while increasing the camera base. It was found that there is a linear relationship between imaging scale and object point precision. Even though the amount of experimental data to compute the standard deviation of 3D-coordinates was small, it was used as an indicator of the previous relationships because the computed interior and exterior calibration parameters were used to compute the 3D-coordinates. The standard deviation values of 3-D coordinates were in the range of (0.001-0.006) cm.

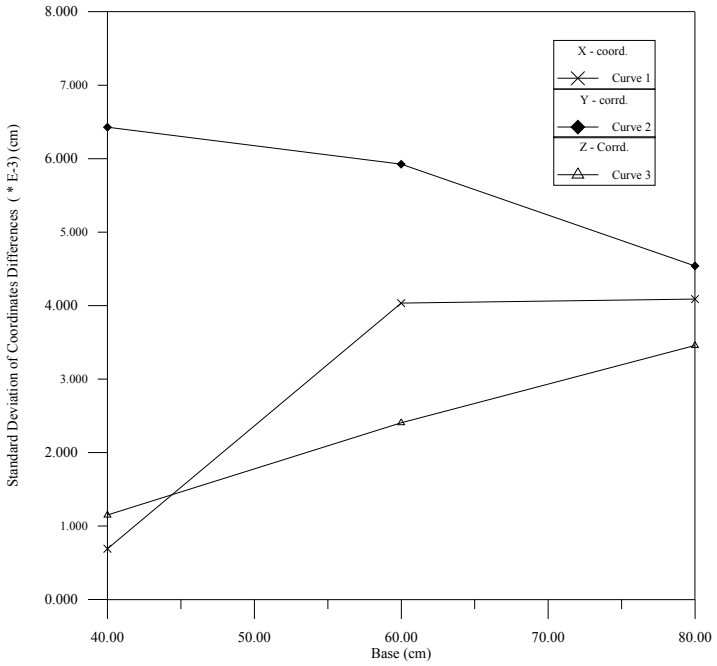

Figure (4): Standard deviations of computed 3-D coordinates for different configurations

SUMMARY AND CONCLUDING REMARKS

Combinations of commonly used base to focal length ratios representing camera configurations were investigated in order to study their effects on modeling the interior geometry of camera lens and their potential accuracy in 3-D computations utilizing a planar object calibration facility. The study was carried out using camera bases that ranged from 40 to 80 cm and pixel sizes between 1.0 and 4.35 mm. A planar facility and a stereo camera rolling platform setup were designed specifically to implement this research work. Least-square mathematical model and computer software were developed to calibrate CCD-cameras using four control

distances only. The distortion model used proved to be reliable and effective.

The findings of this study indicated that increasing the *b/f* ratio to an optimal ratio ranging from 20 to 70 could precisely model the passage of light passing through the lens. At this configuration, the precision of calibration and planar object parameters, the residuals of image points and control distances, the variance-covariance matrices for the unknowns, the precision of the computed 3-D object space points, the values of the standard errors of unit weight and the number of iterations of least-square algorithm were consistent and reliable. Increasing the base at constant focal setting; i.e., increasing the *b/f* ratio, decreased the standard deviations of the computed interior orientation parameters.

In conclusion, the experimental study showed that increasing the *b/f* ratio was more effective to converge the developed least-square model in order to find optimal values for principal distance, affine scaling parameter, radial and decentering distortion parameters, calibration object coefficients in the direction of the plane more than the object depth and computed 3-D object point coordinates.

Despite the promising findings of this study, the results might be enhanced if proper matching algorithm would be utilized to automatically find conjugate image points used for calibration purpose in real time. Further, robust blunders' detection procedure for image measurements and artificial intelligence schemes should be incorporated in order to enhance the automation scheme and decision-making process in modeling the passage of light which passes through the camera lens. Exploring a wider range of *b/f* ratio would also be required in order to find a practical stereo camera configuration. These areas deserve further study.

ACKNOWLEDGEMENT

The author acknowledges and appreciates the support of Jordan University of Science and Technology (JUST) of this research that was carried out during his 2012/2013 sabbatical leave work at the University of Jordan.

REFERENCES

Abraham, S., and Förstner, W. (2005). **"**Fish-eye-stereo calibration and epipolar rectification". ISPRS Journal of Photogrammetry and Remote Sensing, 59 (5), 278-288.

Bleyer, M., and Gelautz, M. (2005). **"**A layered stereo matching algorithm using image segmentation and global visibility constraints". ISPRS Journal of Photogrammetry and Remote Sensing, 59 (3), 128-150.

Brown, D.C. (1971). "Close-range camera calibration". Photogrammetric Engineering, 37 (3), 855-866.

El-Hakim, S. F., Burner, A. W., and Real, R. R. (1989). "Video technology and real-time photogrammetry". Non-topographic Photogrammetry, 2nd Ed., Am. Soc. of Photogrammetry and Remote Sensing, Falls Church, Va., 279-304.

Faig, W. (1989). "Non-metric and semi-metric cameras: data reduction". Non-topographic Photogrammetry, 2nd Ed., Am. Soc. of Photogrammetry and Remote Sensing, Falls Church, Va., 71-79.

Felus, Y. (2004). "Application of total least squares for spatial point process analysis". Journal of Surveying Engineering, ASCE, 130 (3), 126-133.

Fraser, C. S., and Veress, S.A. (1980). "Self-calibration of a fixed-frame multiple-camera system". Photogrammetric Engineering and Remote Sensing, 46 (11), 1439-1445.

Fryer, J.G. (1989). "Camera calibration in non-topographic photogrammetry". Non-topographic Photogrammetry, 2nd Ed., Am. Soc. of Photogrammetry and Remote Sensing, Falls Church, Va., 59-70.

Honda, K., and Nagai, M. (2002). "Real-time volcano activity mapping using ground-based digital imagery". ISPRS Journal of Photogrammetry and Remote Sensing, 57 (1-2), 159-168.

Kratky, V. (1989). "On-line non-topographic photogrammetry". Non-topographic Photogrammetry, 2nd Ed., Am. Soc. of Photogrammetry and Remote Sensing, Falls Church, Va., 107-127.

Obaidat, M.T., and Al-Masaeid, H. (1998). "Video system to monitor archaeological sites using ground-based photogrammetry". ASCE Journal of Surveying Engineering, 124 (1), 3-25.

Obaidat, M.T., and Wong, K.W. (1996). "Geometric calibration of CCD-camera using planar object". ASCE Journal of Surveying Engineering, 122 (3), 97-113.

Pekelsky, J., and Wijk, M.C. (1989). "Moire topography: systems and applications". Non-topographic Photogrammetry, 2nd Ed., Am. Soc. of Photogrammetry and Remote Sensing, Falls Church, Va., 395-430.

Wolf, P.R. (2002). "Surveying and mapping: history, current status and future projections". ASCE Journal of Surveying Engineering, 128 (3), 79-107.

Wong, K.W. (1980). "Basic mathematics of photogrammetry". Manual of Photogrammetry, 4th Ed., Am. Soc. of Photogrammetry, Falls Church, Va., 37-102.

Wong, K.W., Anthony, G.W., and Lew, M. (1989). "GPS-guided vision systems for real-time surveying". ASCE Journal of Surveying Engineering, 115 (2), 243-251.